

## Origin of the metallic field effect\*

A. Berman<sup>†</sup> and H. J. Juretschke

*Polytechnic Institute of New York, Brooklyn, New York 11201*

(Received 30 October 1974)

The electric field effect of epitaxial silver films on mica in vacuum is studied as a function of temperature, thickness, and surface specularity. Attempts to interpret the data in terms of field-induced changes in carrier density, in film thickness, or in surface scattering, each modified by a size effect, lead to the conclusion that the predominant mechanism for altering the thin-film conductance is the change in surface scattering due to surface charging of the interface. This result is independent of the details of the size-effect model used. It implies field-induced changes in surface specularity of order  $10^{-5}$  that decrease with temperature. It also suggests that conduction electrons in silver sense a normally highly positively charged silver-mica interface.

### I. INTRODUCTION

The metallic field effect (MFE) is the change of conductivity of a metallic sample with electrostatic charging. It is usually measured by observing the change of conductance of a thin film forming one plate of a capacitor when the capacitor is charged. For a thin film of conductivity  $\sigma$  and thickness  $t$  the unit area conductance is  $\Sigma = \sigma t$ . If the added charge per unit surface  $q$  is assumed to contribute uniformly to the density of charge carriers throughout the film thickness, the MFE measures the carrier mobility  $\mu$ ,

$$\frac{d\Sigma}{dq} = \frac{d\sigma}{d(q/t)} = \mu, \quad (1)$$

apart from factors of order unity that depend on the change of Fermi level and phonon scattering with carrier density. Hence  $\mu$  is a natural measure of the strength of the field effect. Silver has a room-temperature bulk mobility  $\mu_{\text{bulk}} = 6.4 \times 10^{-3} \Omega^{-1}/(\text{C}/\text{m}^2)$ . If deposited on a substrate of mica, which also acts as the dielectric of a parallel plane capacitor, silver can be given a surface charge of the order of  $2 \times 10^{-3} \text{C}/\text{m}^2$ . Hence its expected change of conductance is  $1.3 \times 10^{-5} \Omega^{-1}$ . In a silver film of  $t = 1000 \text{\AA}$  this amounts to less than one part in  $10^5$ . Hence the MFE is small and requires careful techniques of measurement that avoid extraneous perturbations of  $\Sigma$  of equal or larger magnitude.

Past studies of the MFE<sup>1</sup> in noble metals have mainly confirmed the order of magnitude predicted by Eq. (1), but they have not considered a number of aspects of its physics that are essential. First, in the range of thickness of the samples in which the MFE is measurable, of the order of a mean free path, all transport phenomena such as the conductance, as well as the field effect itself, are modified by size effects. Second, since the surface charge added to a metal resides entirely on

the immediate surface of the sample the model underlying Eq. (1) must be modified to treat a highly localized increase or decrease in charge carriers. In addition, of course, other mechanisms beside the change of density of charge carriers may also be operative.

We have carried out a systematic study of the MFE of epitaxial films of silver on mica in order to clarify these points, and to establish its dominant mechanism.<sup>2</sup> The field-effect measurements have been made on thin-film samples whose bulk and surface transport properties were established by exhaustive size-effect analysis,<sup>3</sup> and the field-effect data have been interpreted in terms of alternate mechanisms, each separately subject to size-effect modification. In fact, the size-effect dependence of the various mechanisms is sufficiently different so that it alone can serve as a guide in deciding between them. Furthermore, the size dependence of all MFE mechanisms is a sensitive function of the theoretical model used for predicting size effects; so much so, in fact, that the observed MFE, taken together with the conductance  $\Sigma$ , can be used to discard certain size-effect theories, something that is not possible on the basis of conductance studies alone.

A preliminary report of our findings has been presented earlier,<sup>4</sup> and some of the consequences of the operative mechanism we have identified have already been verified.<sup>5</sup> This more detailed report will present the experimental data, and will emphasize points of experimental procedure and data analysis that are important in reaching these conclusions.

The analysis considers three possible mechanisms of the MFE for which first-order theoretical models are available. The MFE due to the *change of local carrier density* induced by the surface charge has been discussed in two calculations<sup>6,7</sup> giving differing results. The conflict, if any, between these two results has not been re-

solved, and it may be that they actually deal with different aspects of the same problem. Both versions will be applied to the data. A second mechanism takes into account that the strong electric field in the film surface *alters the effective film thickness*,<sup>6</sup> and thus causes changes in  $\Sigma$  essentially for the same reason that field penetration affects thin-film capacitance.<sup>8</sup> The third mechanism ascribes the MFE to *changes in surface scattering*,<sup>6</sup> caused either directly by the added stationary surface charge, or by the fact that the strong electric field alters the exposed roughness of the existing surface and thus produces changes in specularity of electron-surface collisions.

Simple estimates indicate that any one of these mechanisms could produce results of the observed magnitude. In order to differentiate between them, we must consider the dependence of the various mechanisms on other experimentally accessible parameters entering into the problem. Our experiments have been designed to use for this purpose the parameters of the size effect. Basically, these parameters are  $K$ , the ratio of film thickness  $t$  to bulk mean free path  $\lambda$  and two functions characterizing the electron-surface collisions on the two film surfaces. In the Fuchs-Sondheimer formulation of size effects, for example, these are given by the surface specularity parameters  $P$  and  $Q$ .<sup>6,9</sup> Two such functions are required because in the typical experiment the film surface abutting the mica substrate may have properties differing from those of the film surface facing the vacuum. In the experiments,  $K$  is varied both by using films of different thickness  $t$ , and by making measurements on a given film over a large range of temperatures.  $P$  is varied by artificially creating a rough or smooth outer film surface on the same films, as described in Berman and Juretschke<sup>3</sup> (this paper will be referred to in the text as BJ). The properties of the metal-mica surface, described by  $Q$ , remain the same under variations of  $t$  and  $P$  (and perhaps of  $\lambda$ ). This is the interface subjected to the surface charge of the MFE. Since the conductance data alone define  $K, P$ , and  $Q$  (or their equivalents in other models) fairly uniquely at all temperatures,<sup>3</sup> we can test the MFE data for the different mechanisms in terms of their change with known changes in size-effect parameters. The intrinsic strength of any one mechanism must remain constant under all variations that do not alter the interface, and if this condition has to be satisfied by a sufficiently extensive set of data, its stringency can successfully differentiate between different mechanisms. One inherent difficulty in this procedure, brought out by the results of BJ, is that different theoretical models of size effects assign different sets of parameters to the

conductance data. It is a surprising result of the analysis that our conclusions are insensitive to this ambiguity in all those cases where solutions can be found.

The samples used in this study are the same as those described and discussed in BJ. In fact, since field-effect measurements were taken concurrently with those of  $\Sigma$ , the correlation of both sets of data can fully rely on the common state of the film at any one time. In Sec. II we formulate the size-effect factors of the MFE for the various mechanisms, and list explicit values applying to the six samples at various temperatures, and for different models of size effects.

Section III summarizes experimental aspects of the measurement of the field effect, and displays typical results. Interpretation of the data is taken up in Secs. IV and V.

## II. SIZE-EFFECT FACTORS OF THE MFE

Since the MFE is a small perturbation of the film conductance  $\Sigma$ , it can be written as a first-order expansion about the unperturbed state. In the Fuchs-Sondheimer model,  $\Sigma$ , is a function of the charge density  $n$ , the thickness  $t$ , and the surface specularities  $P$  and  $Q$ . Hence the MFE at the surface described by  $Q$  is

$$\frac{d\Sigma}{dq} = \left( \frac{\partial \Sigma}{\partial t} \right)_{P,Q,n} \frac{dt}{dq} + \left( \frac{\partial \Sigma}{\partial Q} \right)_{P,t,n} \frac{dQ}{dq} + \left( \frac{\partial \Sigma}{\partial n} \right)_{P,t,Q} \frac{dn}{dq}, \quad (2)$$

giving a linear superposition of the three mechanisms described in Sec. I. The three partial derivatives of Eq. (2) are evaluated from the explicit form of  $\Sigma$ . Thus, for the first two we use the Fuchs-Sondheimer formula,

$$\Sigma = \sigma_{\text{bulk}} t f(K; P, Q), \quad (3)$$

where  $f$  has the form given by Eq. (3) of BJ. The third derivative, which requires a new solution of the Boltzmann equation, has been evaluated in two versions,<sup>6,7</sup> for the case  $P = Q$ .

To exhibit the size-effect factors of the MFE explicitly, we rewrite Eq. (2) in the reduced form

$$\frac{1}{\mu_{\text{bulk}}} \frac{d\Sigma}{dq} = F_t A_t + F_Q A_Q + F_n A_n, \quad (4)$$

where the  $A$ 's denote the intrinsic strength of each mechanism and the  $F$ 's are the modifiers due to the size effect. Thus, for example, if  $\sigma_{\text{bulk}} = n_0 e \mu_{\text{bulk}}$  in Eq. (3), we have

$$F_t = f(K; P, Q) + K \left( \frac{\partial f}{\partial K} \right)_{P,Q}, \quad A_t = n_0 e \frac{dt}{dq}, \quad (5)$$

where for large  $t$ ,  $F_t$  approaches unity. Similarly,

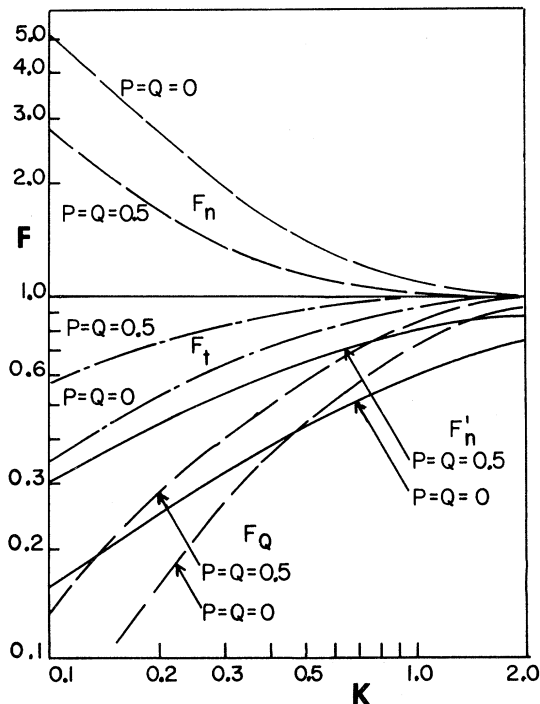


FIG. 1. Theoretical size-effect parameters  $F$  for four mechanisms of the MFE, as a function of the relative film thickness  $K = t/\lambda_{\text{bulk}}$ .

Refs. 6 and 7 define  $F_n$ , with  $A_n=1$  [as expected from Eq. (1)]. For the middle term in Eq. (4), the corresponding separation yields the two factors

$$F_Q = \frac{16}{3} K \left( \frac{\partial f}{\partial Q} \right)_{K,P}, \quad A_Q = \frac{3}{16} n_0 e \lambda_{\text{bulk}} \frac{dQ}{dq}. \quad (6)$$

Thus,  $A_Q$  includes a proportionality to  $\lambda_{\text{bulk}}$ , which will introduce an extraneous temperature dependence in this strength.

All size-effect factors  $F$  show simple monotonic behavior as a function of  $K$ , and, obviously, they differ increasingly from unity as  $P$  and  $Q$  drop below one. Figure 1 shows the extreme size effects expected for  $(P, Q) = (0, 0)$ , and also more typical values for  $(P, Q) = (0.5, 0.5)$ . This figure includes both  $F_n$  and  $F'_n$ , the two separate size effect factors of the two competing models for the MFE based on changes in carrier density.

Table I of BJ gives the full set of parameters ( $K; P, Q$ ) for each film in this study, at five different temperatures. Hence, we can analyze the field-effect data of the six films at these temperatures, since we know absolutely all the size-effect factors  $F$  involved. A complete listing of these factors is given in Table I, for the four lowest temperatures. In the case of  $F_n$  and  $F'_n$ , where only the theory for  $P = Q$  is available, the specularity parameter was chosen as  $\frac{1}{2}(P + Q)$ , a value which is quite adequate for defining  $\Sigma$  well over a large range of  $K$ .<sup>10</sup> The bulk mobility  $\mu_{\text{bulk}}$ , based on one electron per atom, is also included.

Table II provides a similar listing of the size effects to be expected if surface scattering is described by the  $\theta$ -cutoff model of Parrott<sup>11</sup> and Brandli and Cotti.<sup>12</sup> The size effects of the MFE expected in this case have been computed for  $F_t$ ,  $F_Q$ , and  $F_n$ ,<sup>13</sup> and the values in Table II are based on the parameters derived in Table II of BJ. For evaluating  $F_n$ , use is made of the correspondence

$$P \leftrightarrow \sin^4 \theta_P, \quad Q \leftrightarrow \sin^4 \theta_Q, \quad (7)$$

TABLE I. Size-effect factors for four mechanisms of the MFE, evaluated in the isotropic Fuchs-Sondheimer model for the parameter sets characterizing the thin films of this study, at four temperatures.

$T$ (°K) =		100		150		200		250	
$\mu_{\text{bulk}} [10^{-3} \Omega^{-1}/(\text{C}/\text{m}^2)] =$		26.6		15.0		10.3		7.87	
$t$ (Å)		$r$	$s$	$r$	$s$	$r$	$s$	$r$	$s$
290	$F_t$	0.441	0.640	0.620	0.784	0.747	0.877	0.834	0.926
	$F_Q$	0.093	0.229	0.217	0.429	0.323	0.562	0.406	0.634
	$F_n$	3.63	2.01	2.07	1.46	1.53	1.22	1.29	1.11
	$F'_n$	0.185	0.382	0.282	0.471	0.378	0.569	0.407	0.645
690	$F_t$	0.673	0.854	0.835	0.945	0.916	0.975	0.962	0.988
	$F_Q$	0.290	0.556	0.520	0.797	0.661	0.877	0.771	0.910
	$F_n$	1.77	1.25	1.25	1.08	1.03	1.03	1.01	1.01
	$F'_n$	0.301	0.553	0.412	0.655	0.506	0.728	0.590	0.783
1100	$F_t$	0.786	0.929	0.920	0.987	0.967	0.995	0.980	0.998
	$F_Q$	0.454	0.741	0.718	0.946	0.836	0.967	0.901	0.986
	$F_n$	1.36	1.11	1.09	1.02	1.03	1.01	1.01	1.00
	$F'_n$	0.366	0.631	0.473	0.743	0.557	0.797	0.626	0.863

TABLE II. Size-effect factor for three mechanisms of the MFE, evaluated in the Parrott-Cotti model for the parameter sets characterizing the thin films of this study, at four temperatures.

$T$ (°K) =		100		150		200		250	
$\mu_{\text{bulk}} [10^{-3} \Omega^{-1}/(\text{C}/\text{m}^2)] =$		29.1		13.5		9.85		7.62	
$t$ (Å)		$r$	$s$	$r$	$s$	$r$	$s$	$r$	$s$
290	$F_t$	0.423	0.603	0.613	0.794	0.727	0.845	0.800	0.878
	$F_Q$	0.986	0.986	0.948	1.00	0.629	0.953	0.175	0.269
	$F_n$	3.89	1.16	2.04	1.12	1.49	1.14	1.30	1.11
690	$F_t$	0.655	0.831	0.837	0.952	0.890	0.974	0.945	0.992
	$F_Q$	0.968	0.968	1.00	1.00	0.940	1.00	0.260	0.275
	$F_n$	1.83	1.12	1.24	1.06	1.14	1.04	1.06	1.02
1100	$F_t$	0.773	0.916	0.923	0.986	0.962	0.996	0.981	0.999
	$F_Q$	0.992	0.992	0.951	1.00	0.994	1.00	0.282	0.284
	$F_n$	1.40	1.09	1.08	1.04	1.03	1.02	1.02	1.01

which relates many features of the two size-effect models.

Finally, Table III lists the size-effect parameters of the MFE for the third model of the conductivity of silver explored in BJ, which takes into account the anisotropy of the Fermi surface of silver, and assigns all size effects to the belly electrons. Assuming that only the belly electrons contribute to the MFE, justified if the neck electrons have little interaction with the surface, we must also apply a modified normalization for the field-effect data. Guessing that  $n_{\text{neck}}/n_{\text{belly}} = \frac{1}{9}$ , for the necks important in our geometry, we require that  $\mu_{\text{belly}}/\mu_{\text{bulk}} = \frac{10}{9}(\sigma_B^0/\sigma_B)$ . This normalization is also indicated in Table III.

### III. EXPERIMENTAL SUMMARY

The sample preparation and characterization, and the over-all design of the experimental sequence to produce overlapping data on a set of films with well-defined bulk and surface properties have been described extensively in BJ. The circuits for the electrical measurements of the MFE are given in block form in Fig. 2.

A dc current of several mA from a constant current source traverses the sample, and both  $I$  and  $V$  are recorded, to determine the film resistance  $R$ . When a 500-Hz voltage  $V_1$  of up to 100 V(rms) is applied across the mica, the voltage  $V$  acquires a ripple  $\delta V$  at this frequency, which is amplified and detected by a phase sensitive detec-

TABLE III. Size-effect factors of four mechanisms of the MFE, evaluated in the anisotropic two-carrier Fuchs-Sondheimer model for the parameter sets characterizing the thin films of this study, at four temperatures. The bulk mobility of the belly electrons of silver is also listed.

$T$ (°K) =		100		150		200		250	
$\mu_{\text{bulk}}^{(b)} [10^{-3} \Omega^{-1}(\text{C}/\text{m}^2)] =$		28.6		15.7		10.5		7.82	
$t$ (Å)		$r$	$s$	$r$	$s$	$r$	$s$	$r$	$s$
290	$F_t$	0.458	0.659	0.601	0.796	0.703	0.876	0.778	0.929
	$F_Q$	0.104	0.268	0.219	0.481	0.326	0.625	0.431	0.732
	$F_n$	3.42	1.92	2.15	1.39	1.65	1.21	1.39	1.19
	$F_h$	0.193	0.395	0.263	0.503	0.318	0.574	0.361	0.625
690	$F_t$	0.681	0.860	0.826	0.949	0.896	0.979	0.938	0.991
	$F_Q$	0.298	0.590	0.525	0.820	0.675	0.914	0.788	0.964
	$F_n$	1.74	1.24	1.27	1.08	1.13	1.03	1.06	1.02
	$F_h$	0.306	0.559	0.391	0.658	0.438	0.703	0.468	0.731
1100	$F_t$	0.800	0.936	0.916	0.985	0.960	0.995	0.981	0.999
	$F_Q$	0.468	0.765	0.834	0.918	0.836	0.960	0.910	0.976
	$F_n$	1.33	1.10	1.10	1.02	1.04	1.01	1.02	1.00
	$F_h$	0.375	0.639	0.452	0.716	0.486	0.746	0.504	0.760

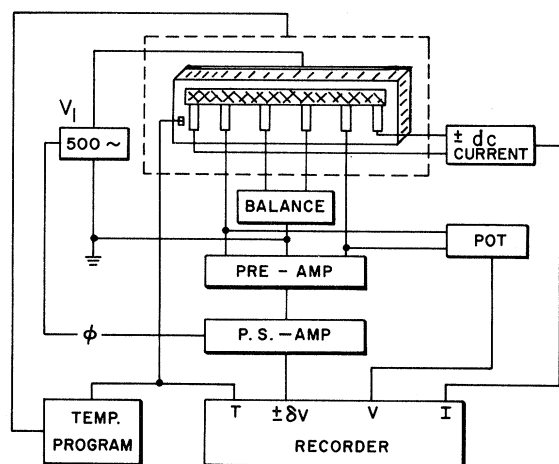


FIG. 2. Block diagram of the electrical circuits for measuring the metallic field effect.

tor. Since ruby muscovite mica is centrosymmetric, there is no piezoelectrically strain-induced contribution to the change in resistance. A balance circuit nulls out any asymmetries in the charging current of the parallel-plate capacitor which would give a 500-Hz signal even when  $I=0$ . During the measurement, the current  $I$  is reversed every three minutes, and the field-effect signal is taken as  $\frac{1}{2}[\delta V(+I) - \delta V(-I)]$ . This value remains insensitive to small drifts in the balance.

Before accepting a set of field-effect data from a sample, we require that  $\delta V$  be linearly proportional to both  $I$  and  $V_1$  and that  $\delta V(\pm I)$  is symmetric with respect to  $\delta V(0)$ . To achieve this symmetry it is imperative that ground loops are eliminated by carefully centering the electrical ground throughout all stages of detection. We have found no phase shift between  $V_1$  and the field-effect signal. The amplifying system is calibrated by a known signal reduced by a voltage divider to give output levels comparable to  $\delta V$ . The recorder gives a full scale deflection of 100 divisions at an input of  $10^{-7}$  V.

A thermocouple mounted on the sample provides the input to the temperature programmer, moving the temperature between 100 and 600°K at a predetermined rate of about 0.5°K per minute. Relays switch the recorder between  $T$ ,  $I$ ,  $V$ , and  $\delta V(\pm I)$  every six minutes, and the calibration is checked throughout each run.

The specific surface charge  $q$  is related to  $V_1$  through the sample capacitance corrected for the area contributed by the contacts. A typical sample capacitance was  $2 \times 10^{-9}$  F, leading at  $V_1 = 100$  V to  $q \approx 1.4 \times 10^{-3}$  C/m<sup>2</sup>.

The absolute sign of the field effect was checked

by tracing all phase shifts within the detection system. It is such that in silver the sample conductance  $\Sigma$  increases when electrons are added to the interface. Thus,  $d\Sigma/dq$  is negative. Given the errors in all the auxiliary measurements, as well as fluctuations in amplifier calibration, we estimate the absolute magnitudes of  $d\Sigma/dq$  to be determinable within (10–15)%. Reproducibility of a given point, and of the relation of adjacent points, as the temperature is varied, is within one-third of this spread.

A typical measurement of the field effect  $dR/dq$  as a function of temperature is shown in Fig. 3. These data accompany those of Fig. 3 of BJ, and they show the strong decrease in the field effect when the surface conditions of the outer surface are changed. Data points corresponding to the original layer 15Å thinner cannot be distinguished from those of the annealed state of 290Å. It is interesting to note that in the temperature range in which the surface anneals, the MFE reaches its annealed value at a temperature about 50°K above that at which the resistivity (Fig. 3, BJ) indicates completion of the annealing process. Apparently here the field effect is more sensitive to details of the surface condition than the resistance or than the description provided by simple specular parameters. It is for this reason that the MFE analysis is not carried into the temperature range where surface annealing occurs.

#### IV. RESULTS AND ANALYSIS

A complete set of smoothed-out results of the field-effect conductance  $d\Sigma/dq$  as a function of temperature for the six films included in this study is presented in Fig. 4. These data were taken simultaneously with the corresponding resistivities of Fig. 4 of BJ. At all thicknesses the MFE is much bigger if the outer surface is smooth rather than rough. The increase of the MFE at lower temperatures largely reflects the increase in the bulk mobility, but the thinner films show less of an increase, most likely because for them the size-effect modification becomes most severe.

Figure 5 presents the same data normalized to  $\mu_{\text{bulk}}$  and plotted versus the  $K$  values of the isotropic Sondheimer model (Table I of BJ). Since both scales are logarithmic, this representation is, in fact, insensitive to the choice of  $\mu_{\text{bulk}}$ , or to other constant factors, and therefore applies equally to all size-effect models. That size effects indeed play a role in the interpretation of the data is clearly brought out in Fig. 5. As  $K$  increases,  $d\Sigma/dq$  of all films tends towards a common value independently of thickness or surface condition. This value is of order unity, indicating that the

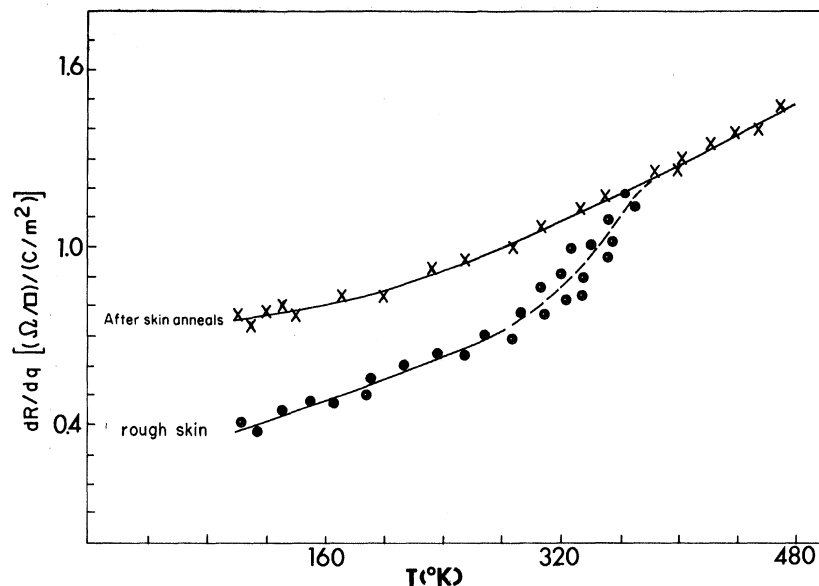


FIG. 3. Specific field-effect resistance  $dR/dq$  as a function of temperature of a 290-Å silver film on mica. The two low-temperature branches refer to the two states of the outer surface of the silver film.

choice of normalization suggested by Eq. (1) is useful. As  $K$  decreases, the films showing the largest deviation from the asymptotic value are those with rough surfaces, where size effects are expected to be most pronounced. It is interesting to observe that while most trends of small- $K$  behavior are towards decreases in  $d\Sigma/dq$ , the thickest films with smooth surface show the opposite behavior. Thus both trends predicted in Fig. 1 appear in the data.

The fact that the two families of films with either rough or smooth outer surface do not fall onto a universal curve is not surprising in view of the

results of BJ, where it was found that the surface specularities are also temperature dependent.

Therefore, a separate analysis at each temperature is required. Figure 5 indicates explicitly the points corresponding to 100, 150, 200, 250, 300, and 350° K. The four lowest temperatures, available for all films, will be analyzed in detail. For convenience, the normalized MFE at these temperatures is tabulated in Table IV, as derived from the smoothed-out curves of Fig. 5.

The analysis of these data proceeds according to Eq. (4). Given a particular model of size effects, we know the size factors for any one mecha-

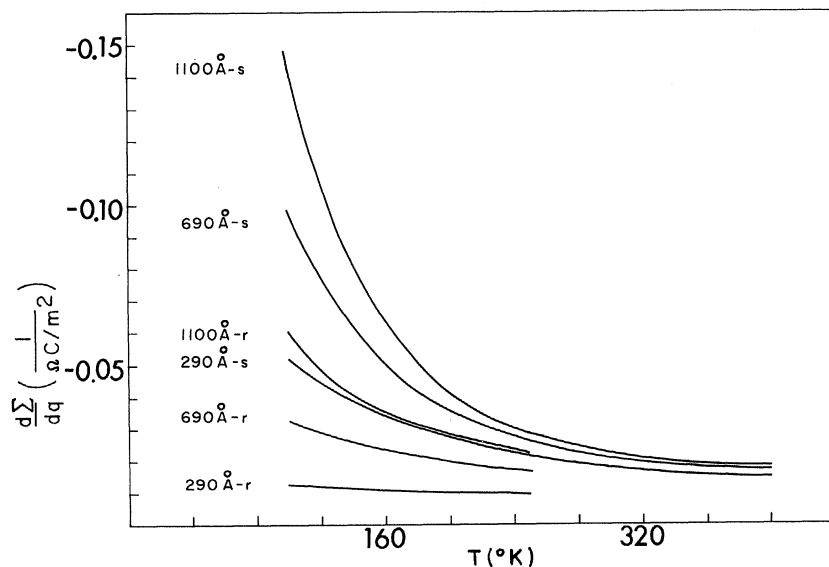


FIG. 4. Specific field-effect conductance of three silver films of different thicknesses, for both the rough ( $r$ ) and smooth ( $s$ ) states of the outer surface of the film.

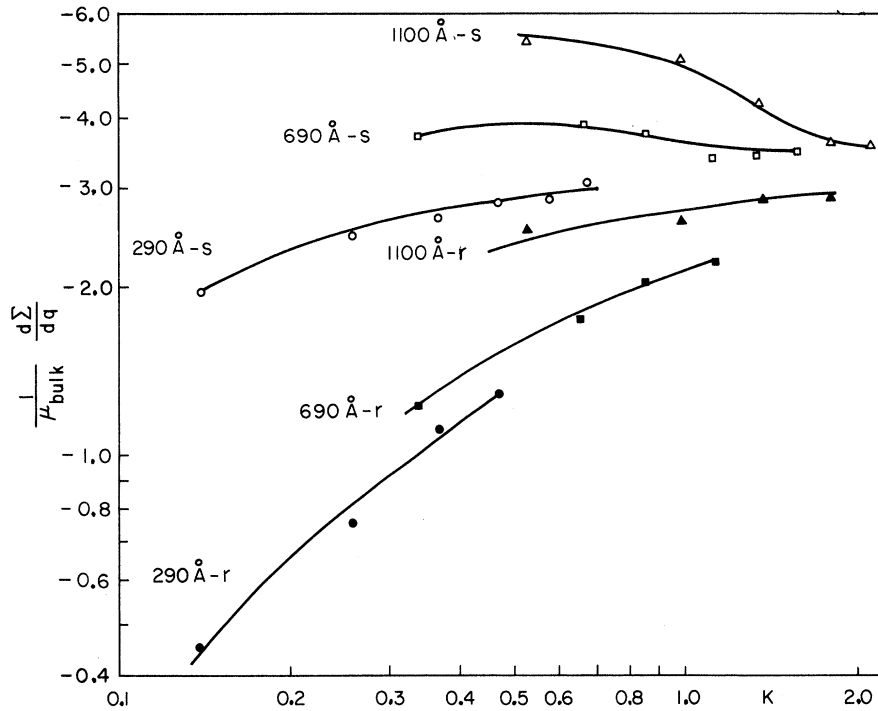


FIG. 5. Data of Fig. 4 normalized to the bulk mobility  $\mu_{\text{bulk}}$ . The  $K$  values are assigned according to Table I of BJ.

nism, such as for example  $F_Q$ , for all six films at the given temperature. The unknown strength  $A_Q$  must be common to all six data, since the silver-mica interface characterized by  $Q$  remains the same throughout the experiment. We can therefore find  $A_Q$  by a best fit of the data of Table IV combined with the information of Table I. The same fitting process can be repeated in searching for  $A_t$ ,  $A_n$ , and  $A'_n$ , and, indeed, any linear combination including up to all four mechanisms. A test of whether any such solution is physically meaningful requires that the rms deviation of computed points from experimental points be small, that the trend of the experimental points is reproduced, and that the solution is insensitive to variations of the experimental input within the uncertainty of the data, or to the number of points chosen. Since the experimental data span more

than one magnitude, we have chosen to minimize the mean-square fractional deviation of all points.

For the isotropic Fuchs-Sondheimer model of size effects, the above criteria are satisfied only by the charge scattering mechanism described by  $A_Q$ . Table V lists the strengths  $A_Q$  at the four temperatures, and the theoretical fit for all six data at each temperature. Comparison with Table IV shows that the trends of all data are well reproduced. The rms deviation of about 20% is distributed uniformly, and the value of  $A_Q$  remains practically the same whether the analysis is based on sets of six or four data points. In contrast, for the three other mechanisms the best fit has an rms deviation between 40 and 80%, the trend of points with temperature is skew, and the solution is very sensitive to the sets of particular points chosen. We conclude that in terms of a single mechanism,

TABLE IV. Experimental data of the reduced MFE  $\mu_{\text{bulk}}^{-1} d\Sigma/dq$  at four different temperatures, for three film thicknesses. For each film, values are listed for the outer surface rough ( $r$ ) and smooth ( $s$ ).

$T$ ( $^{\circ}\text{K}$ ) =	100		150		200		250	
$t$ ( $\text{\AA}$ )	$r$	$s$	$r$	$s$	$r$	$s$	$r$	$s$
290	0.45	1.93	0.80	2.53	1.15	2.75	1.28	2.68
690	1.21	3.68	1.75	3.90	2.02	3.72	2.23	3.30
1100	2.52	5.43	2.62	5.00	2.83	4.19	2.75	3.53

TABLE V. One-parameter fit of data of Table IV, using  $F_Q A_Q$  only, for the isotropic Fuchs-Sondheimer size-effect model.

$T$ ( $^{\circ}\text{K}$ ) =	100		150		200		250	
$A_Q =$	5.49		4.10		3.75		3.31	
$t$ ( $\text{\AA}$ )	$r$	$s$	$r$	$s$	$r$	$s$	$r$	$s$
290	0.51	1.26	0.89	1.76	1.21	2.09	1.34	2.10
690	1.59	3.06	2.15	3.28	2.46	3.27	2.56	3.01
1100	2.48	4.06	2.94	3.88	3.12	3.60	2.99	3.27

only  $A_Q$  gives a physically meaningful fit to the experimental data.

If more than one simultaneous mechanism is included, this conclusion is not altered. Table VI lists the strengths derived in such analysis. All  $A$ 's except  $A_Q$  are very small, and their contributions to the best fit amount to 1% or less at the two highest temperatures, with  $F_n'A_n'$  contributing between 2 and 15% at 150°K. The four-parameter analysis at 100°K gives no stable answer.

The same method of analysis, applied to the  $\theta$ -cutoff model of size effects based on Table II does not produce any solution satisfying the criteria of physical reasonableness. A fit is only achieved by the near cancellation of very large contributions of opposite signs, and is very sensitive to the exact input data.

Finally, the data of Table IV have been analyzed for the two-carrier anisotropic model for silver, using the size-effect factors of Table III. The results are summarized in Table VII. They are substantially the same as those of the isotropic model in Table VI, even though the size-effect factors of the two models are different. The surface scattering mechanism clearly predominates at all temperatures. Only at the lowest temperature could the fit be improved somewhat by including the other mechanisms, although it remains unclear which of these becomes physically meaningful here.

Further analyses, based on the additional modifications of strain and initial thickness for the interpretation of size effects explored in BJ, gave substantially the same results.

## V. DISCUSSION

It is clear from the analysis of Sec. IV that, within the framework of the Fuchs-Sondheimer size effects given by Eqs. (3)–(6), surface scattering modified by the applied electric field is the dominant cause of the MFE, at least in silver on mica. This conclusion remains valid when the data are examined using different interpretations of the bulk conduction properties of the silver films, such as isotropic or anisotropic conduction, a strain-dependent contribution to the resistivity,

TABLE VI. Strengths of four mechanisms by four-parameter fit of the data of Tables I and IV for the isotropic Fuchs-Sondheimer model, at three temperatures.

$T$ (°K) =	150	200	250
$A_t$	−0.007	−0.004	−0.004
$A_Q$	4.26	3.81	3.42
$A_n$	−0.006	−0.006	−0.011
$A_h$	0.025	0.017	0.015

and different effective thicknesses of films with rough surface layers. As shown in BJ, these modifications cause significant changes in the films' surface specularities and their temperature dependence, and since they all interpret the conductance data equally successfully, it is difficult to choose between them. It is surprising that despite these models leading to different descriptions of surface properties, and the corresponding role of size effects they bring to the MFE, the surface scattering mechanism clearly predominates in all cases; if they contribute at all, any of the other mechanisms lie within the noise of our data.

The other clear-cut conclusion of the analysis is that our data cannot be interpreted in terms of the size-effect theory of Parrott and Cotti. This implies that, at a minimum, the straightforward extension of this theory to size effects in the MFE analogous to that given by Eq. (2) is inadequate, or, more seriously, that the approach to size effects of this theory is itself open to question.

It should be noted that our best fit does not reproduce the exact experimental data. Figure 6 compares the numbers of Tables IV and V as a function of temperature. All our theoretical points at a given temperature are derived from the size-effect factors of Table I and a common strength  $A_Q$ . Even though all trends are reproduced, especially those giving variations in opposite directions as the temperature decreases, our best fits invariably give a smaller difference between rough and smooth films than the experiment. The reason for this is not understood, but may reside in such aspects of a more realistic size-effect theory as local fluctuations in surface roughness and in size-effect parameters  $K$  that affect con-

TABLE VII. One-parameter fit of the data of Table IV to the size-effect parameters of Table III of the anisotropic two-carrier model, at four temperatures. The reduced experimental data use the bulk mobility of belly electrons.

$T$ (°K) =	100		150		200		250	
$A_Q =$	4.86		4.05		3.64		3.29	
$t$ (Å)	$r$	$s$	$r$	$s$	$r$	$s$	$r$	$s$
290								
Expt.	0.42	1.80	0.77	2.44	1.13	2.72	1.31	2.91
Fit	0.51	1.30	0.75	1.89	1.15	2.26	1.39	2.39
690								
Expt.	1.14	3.44	1.69	3.65	1.99	3.68	2.27	3.36
Fit	1.45	2.87	2.08	3.35	2.42	3.30	2.58	3.14
1100								
Expt.	2.37	5.09	2.52	4.78	2.80	4.15	2.80	3.60
Fit	2.27	3.72	2.88	3.77	3.02	3.48	2.98	3.20



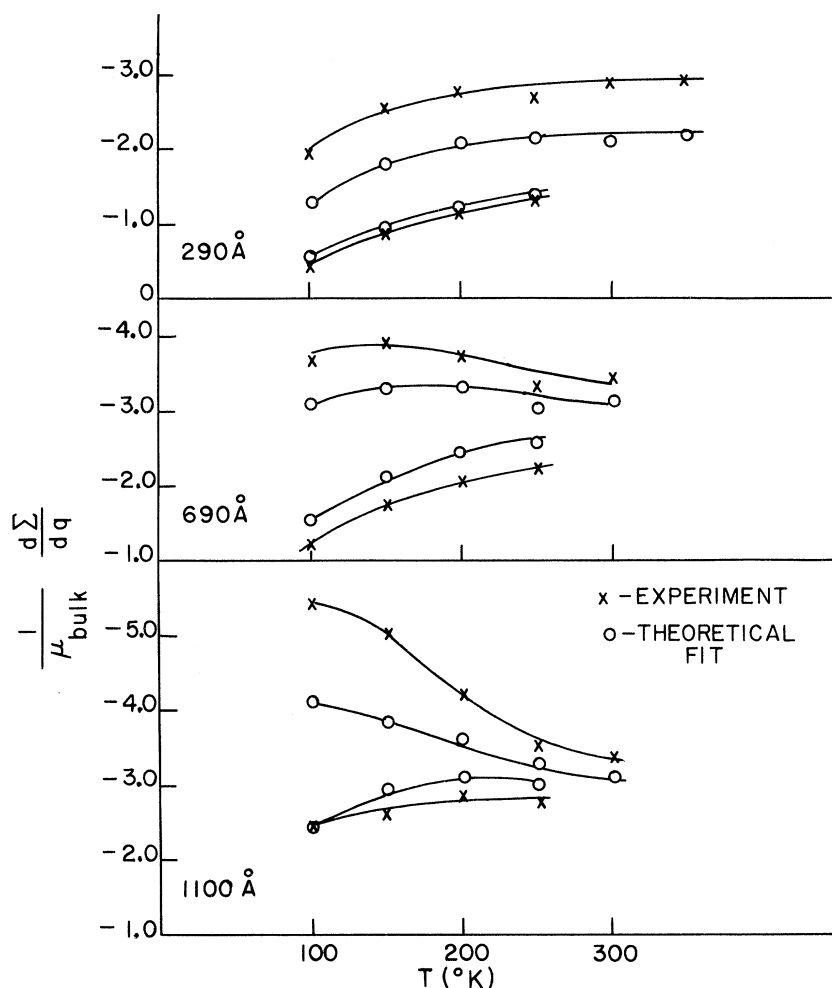


FIG. 6. One-parameter fit of the surface scattering mechanism for the MFE to the experimental data, from Table V. All points at a given temperature have a common strength  $A_Q$ .

ductance and field effect differently.

Our conclusion about the origin of the MFE is in partial agreement with McIrvine's<sup>14</sup> explanation of the MFE on ferroelectric substrates.<sup>15</sup> He found that a change in specularity parameters is required, in addition to the direct transport effect of the added charge (given by  $A_n'$ ). In his formulation, however, the two effects are not additive, and a change in  $Q$  is invoked to explain the observed increase in surface conductivity above bulk value.

Using the data of Table V and Eq. (6), the effectiveness of the charge  $q$  in changing the specularity  $Q$  is known. Figure 7 shows  $dQ/dq$  versus  $T$ , indicating that this effectiveness is linear at low  $T$  and varies like  $\lambda_{\text{bulk}}^{-1}$  at high  $T$ . With a maximum charge of  $2 \times 10^{-3}$  C/m<sup>2</sup>,  $Q$  changes by several parts in  $10^5$ . This makes the MFE a very sensitive probe of surface conditions, but it also implies that a fully quantitative interpretation requires a much more detailed description of sur-

face properties than offered by current size-effect theories.

A straightforward explanation of how the field effect changes  $Q$  assumes that the applied charge  $q$  resides in localized surface centers and causes additional scattering of the conduction electrons. Such scattering mechanisms have been considered by Greene and O'Donnell,<sup>16</sup> McIrvine,<sup>14</sup> and Greene and Malamas.<sup>17</sup> This model implies, however, that the metal-insulator interface is normally charged, since the observed field effect changes sign with the sign of  $q$ , while scattering is independent of the sign of the charge center. Furthermore, this normally resident charge  $q_0$  must be large compared to  $q$ . Using this model we conclude that the silver-mica interface acts for conduction electrons as if it were positively charged to a density large compared to  $2 \times 10^{-3}$  C/m<sup>2</sup>, or more than  $10^{-4}$  electrons/(surface atom). Charges and dipoles at the surface of mica under various conditions of cleavage have already been reported.<sup>18</sup>

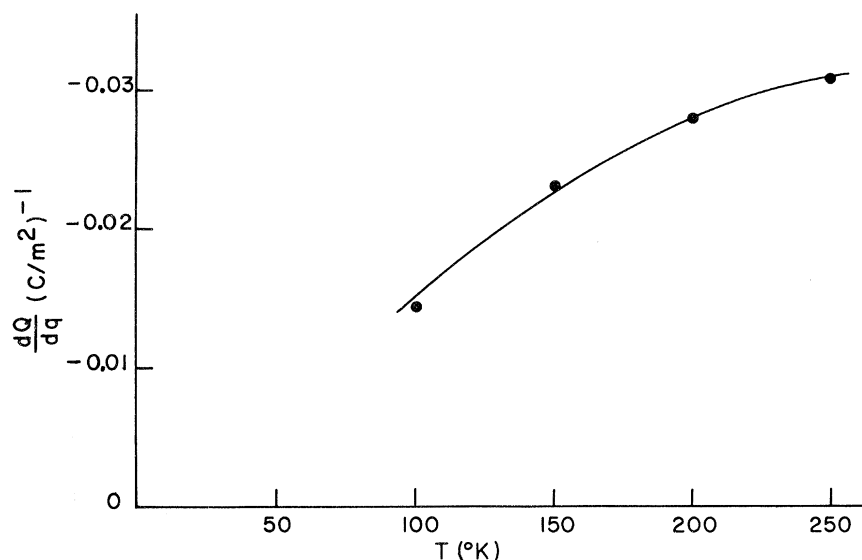


FIG. 7. Effectiveness of surface charge  $q$  in changing surface specularity  $Q$ , at the silver-mica surface, as a function of temperature.

The applied charge  $q$  would then merely alter this already existing state of surface charge.

An alternate proposal ascribes the change of surface scattering to field-controlled tunneling into and out of interface traps by the current carriers.<sup>19</sup> The data presented here are compatible

with either proposal. Some additional experiments, stimulated by predictions of the charge scattering model and interpreted in terms of this model have already been reported,<sup>5</sup> and further results will be given in another publication.

\*Supported in part by the Joint Services Electronics Program, the Office of Naval Research, and the National Science Foundation.

†Present address: Dept. of Phys., New York City Community College, Brooklyn, N.Y. 11201.

<sup>1</sup>A. Deubner and K. Rambke, *Ann. Phys. (Leipz.)* **17**, 317 (1956); G. Bonfiglio and R. Malvano, *Phys. Rev.* **115**, 330 (1959); M. D. Sherrill, Ph.D. thesis (University of North Carolina, 1961) (unpublished); R. E. Glover III and M. D. Sherrill, in *Symposium of Electrical and Magnetic Properties of Thin Metallic Layers* (Academy of Sciences of Belgium, Brussels, 1961), p. 316.

<sup>2</sup>A. Berman, Ph.D. thesis (Polytechnic Institute of Brooklyn, 1970) (unpublished); *Bull. Am. Phys. Soc.* **16**, 144 (1971).

<sup>3</sup>A. Berman and H. J. Juretschke, preceding paper, *Phys. Rev.* **11**, 2893 (1975). This paper will be referred to in the text as BJ.

<sup>4</sup>A. Berman and H. J. Juretschke, *Appl. Phys. Lett.* **18**, 417 (1971). (The present paper also corrects errors in some of the magnitudes reported there.)

<sup>5</sup>H. J. Juretschke and L. Goldstein, *Phys. Rev. Lett.* **29**, 767 (1972).

<sup>6</sup>H. J. Juretschke, *Surf. Sci.* **2**, 40 (1964).

<sup>7</sup>E. C. McIrvine, *Surf. Sci.* **5**, 171 (1966).

<sup>8</sup>A. K. Theophilou and A. Modinos, *Phys. Rev. B* **6**, 801 (1972).

<sup>9</sup>M. S. P. Lucas, *J. Appl. Phys.* **36**, 1632 (1965).

<sup>10</sup>H. J. Juretschke, *J. Appl. Phys.* **37**, 435 (1966).

<sup>11</sup>J. E. Parrott, *Proc. Phys. Soc. Lond.* **85**, 1143 (1965).

<sup>12</sup>G. Brandli and P. Cotti, *Helv. Phys. Acta* **38**, 801 (1965).

<sup>13</sup>H. J. Juretschke, *Surf. Sci.* **5**, 111 (1966).

<sup>14</sup>E. C. McIrvine, *Phys. Rev.* **148**, 148 (1966).

<sup>15</sup>H. L. Stadler, *Phys. Rev. Lett.* **14**, 979 (1965).

<sup>16</sup>R. F. Greene and R. W. O'Donnell, *Phys. Rev.* **147**, 599 (1966).

<sup>17</sup>R. F. Greene and J. Malamas, *Phys. Rev. B* **7**, 1384 (1973).

<sup>18</sup>K. Müller and C. C. Chang, *Surf. Sci.* **14**, 39 (1969).

<sup>19</sup>J. Halbritter, *Phys. Lett. A* **43**, 309 (1973).